

# A FLASH on Blazars

## Capturing the Radio Realm of 4FGL Blazars with SKAO Pathfinders

M. Behiri<sup>1,2,3\*</sup>, E. K. Mahony<sup>4</sup>, E. Sadler<sup>4,5,6</sup>, E. Kerrison<sup>4,5,6</sup>, A. Traina<sup>7</sup>, M. V. Zanchettin<sup>8</sup>, V. Galluzzi<sup>2</sup>, A. Lapi<sup>1,2,3,9</sup>, and M. Massardi<sup>10,1</sup>

<sup>1</sup> Scuola Internazionale Superiore di Studi Avanzati, Via Bonomea 265, 34136 Trieste, Italy

<sup>2</sup> INAF - Istituto di Radioastronomia, Via Gobetti 101, 40129 Bologna, Italy

<sup>3</sup> IFPU - Institute for fundamental physics of the Universe, Via Beirut 2, 34014 Trieste, Italy

<sup>4</sup> ATNF, CSIRO Space and Astronomy, PO Box 76, Epping, NSW 1710, Australia

<sup>5</sup> Sydney Institute for Astronomy, School of Physics A28, University of Sydney, NSW 2006, Australia

<sup>6</sup> ARC Centre of Excellence for All Sky Astrophysics in 3 Dimensions (ASTRO 3D)

<sup>7</sup> INAF-OAS Bologna, via Gobetti 101, I-40129 Bologna, Italy

<sup>8</sup> INAF - Osservatorio Astrofisico di Arcetri, Largo E. Fermi 5, I-50125, Firenze, Italy

<sup>9</sup> INFN, Sezione di Trieste, via Valerio 2, Trieste I-34127, Italy

<sup>10</sup> INAF, Istituto di Radioastronomia, Italian ARC, Via Piero Gobetti 101, I-40129 Bologna, Italy

March 18, 2025

### ABSTRACT

This work investigates the multi-wavelength properties of 165 4FGL blazars from the *Fermi*-LAT fourth source catalogue, looking for with counterparts in the Australian SKA Pathfinder (ASKAP) First Large Absorption Survey in HI (FLASH) continuum. Using high-resolution data from FLASH and complementary radio datasets, combined with archival Atacama Large Millimeter Array (ALMA) observations, we perform detailed spectral energy distribution (SED) analyses across cm-to-mm wavelengths. Our findings reveal that most blazars exhibit re-triggered peaked spectra, indicative of emission dominated by a single emitting region. Additionally, we identify strong correlations between radio and gamma-ray luminosities, highlighting the significant role of relativistic jets in these active galactic nuclei. The inclusion of spectroscopic redshifts from Sloan Digital Sky Survey (SDSS) and Gaia enables a comprehensive analysis of the evolutionary trends and physical characteristics of the sources. Furthermore, we report a tight Radio-X-ray Correlation for Flat Spectrum Radio Quasars, contrasting with the more scattered behaviour observed in BL-Lacs, reflecting their distinct accretion and jet-driving mechanisms. These results provide critical insights into the physics of blazars and their environments, paving the way for future studies with next-generation facilities like the SKA Observatory (SKAO) for radio observations and Cherenkov Telescope Array for gamma-ray studies.

**Key words.** galaxies: active – BL Lacertae objects: general – galaxies: jets – radio continuum: galaxies – gamma rays: galaxies

## 1. Introduction

The latest radio interferometers are opening up a brand new window on the main characters of the radio sky: the Active Galactic Nuclei (AGN). Observatories like the Murchison Wide-field Array (MWA, Tingay et al. 2013) and the Australian SKA Pathfinder (ASKAP) are able to target faint populations at low radio frequencies, efficiently covering wide areas of the sky. The large multi-wavelength statistic of objects surveyed by these telescopes, finally makes it possible to answer several open questions on the physics and the evolutionary role of the different AGN types.

Within the radio spectrum, the primary emission process is synchrotron radiation, resulting from electrons moving at relativistic speeds as they spiral around magnetic field lines. This process is characteristic of radio AGN, producing the distinctive relativistic jets. From the radio Spectral Energy Distribution (SED), it is possible to retrieve clues about the history of the AGN. For instance, an inverted spectrum is a hint for self-absorption processes, typical of compact sources. On the other

end, a break at high radio frequency suggests the presence of ageing processes, while a flat spectrum could be either a hint of efficient energy pumping, continuously refurbishing the jets with energetic electrons, or of the superposition, along the line of sight, of several components. Further, changes in the trend of the SED might be a proxy for reactivation episodes of the AGN. Thus, broad radio spectral coverage is key for reaching a comprehensive view of the radio emission of the AGN.

Among the several classes of AGN, blazars appear rather interesting from a radio point of view. According to the Unified Model by Urry & Padovani (1995), blazars are AGN whose jets are oriented almost ( $< 15\text{-}20$  deg) along the line of sight. They are characterised by Doppler boosting of their flux density, apparent superluminal motion, large and rapid variability, and strong, non-thermal emission over the entire electromagnetic spectrum (Padovani 2016).

Blazars constitute an ideal background target for detecting HI absorption in both the interstellar medium (ISM) and intergalactic medium (IGM), as their intense radio emission enables the detection of absorption at high redshifts, improving our understanding of the distribution and properties of neutral gas in the Universe (e.g., Maina et al. 2022; Srianand et al. 2022). Thus,

\* e-mail: mbehiri@sissa.it

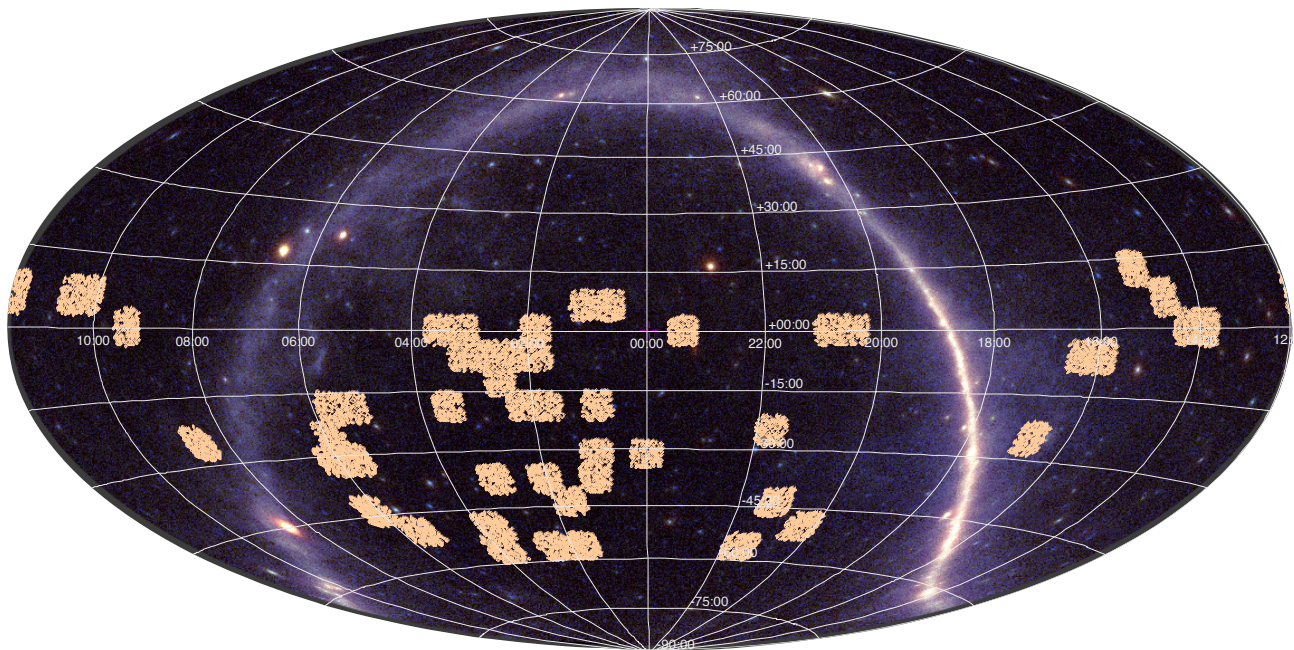


**Fig. 1.** Map showing the coverage of *Fermi*-LAT 4FGL, with the light pink regions representing the MOC (Multi-Order Coverage) of the FLASH fields utilised in this work.

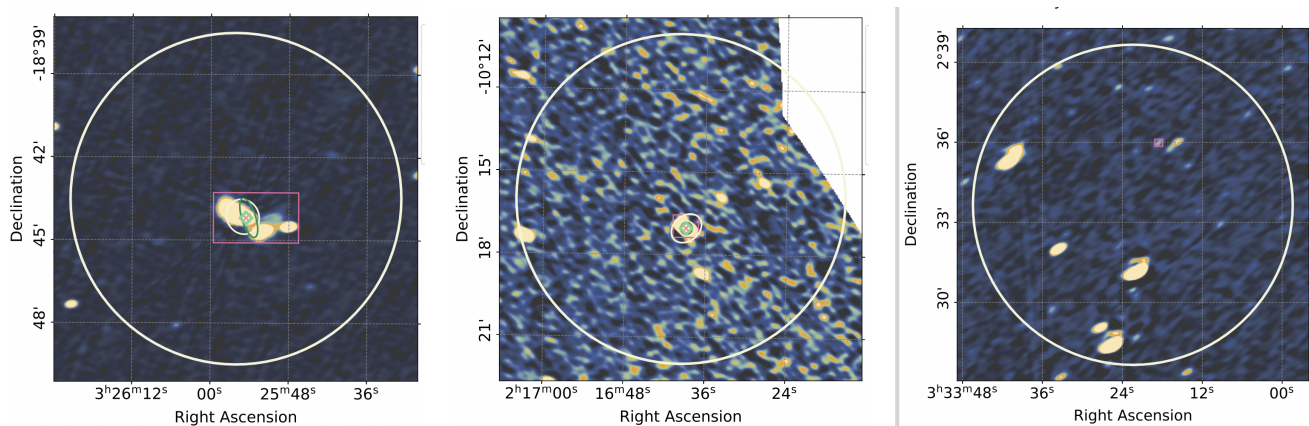


**Fig. 2.** The illustrations show three sources categorized as "IN" (Left), "OUT" (Center), and "UNCERTAIN" (Right), respectively. These images are based on FLASH maps. The large white circle is aligned with the *Fermi*-LAT location, sharing the same radius as the *Fermi*-LAT's resolution (0.1 degrees). The pink rectangle is positioned at the FLASH continuum island's location, with dimensions matching those of the island as determined by SELAVY (Whiting & Humphreys 2012). The dark green ellipse indicates the size and position of the corresponding RACS-LOW island, and the small white circle marks the GLEAM-X matched source's location, with a size equivalent to the (median) GLEAM-X resolution (in arcseconds). The pink "X" and light green diamond denote the best-corresponding positions of the AT20G source to the 4FGL position and the FLASH continuum position, respectively.

projects like the First Large Absorption Survey in HI (FLASH, Yoon et al. 2024), made with the ASKAP, leverage the characteristics of blazars to study HI absorption, neutral gas evolution, and jet-environment interactions. The ability of blazars to illuminate cosmologically distant environments makes them indispensable tools for investigating the distribution of neutral gas and its interaction with relativistic jets. Therefore, ahead of the upcoming data from FLASH and the completion of this survey, a first step towards the full accomplishment of using blazars for HI absorption is, indeed, to understand the peculiarities of the blazar population that FLASH is able to target. Understanding the radio properties of blazars in the FLASH continuum catalogue

is key for exploiting their potential as astrophysical probes. In particular, their strong gamma-ray emission makes gamma-ray selection an effective way to identify and classify them (Abdo et al. 2010; Nolan et al. 2012; Acero et al. 2015; Giroletti et al. 2016). The *Fermi* Large Area Telescope Fourth Source Catalog Data Release 4 (4FGL) by Ballet et al. (2023) offers the perfect playground for identifying blazars. Blazars are, in fact, strong gamma-ray emitters through inverse Compton (IC) of the jet electrons with external photons, typically from the disk, synchrotron self-Compton (SSC) from the same electrons producing the radio emission and hadronic processes. Hadronic processes are generated by protons losing energy through synchrotron

emission (if the magnetic field is large enough) or photo-meson reactions. In the latter case neutrino emission from the decaying charged pions is also expected (Tavecchio 2017; Padovani et al. 2022b,a). In the 4FGL catalogue, blazars are divided into two subclasses:

- **BL-Lacertae objects (BL-Lac, BLL)**, characterised by extremely weak or even absent emission lines in their optical spectra. In these objects, gamma-ray emission is predominantly driven by SSC. Their AGN emission is thought to be mainly driven by the rotation of the supermassive black hole.
- **Flat Spectrum Radio Quasars (FSRQ)**, which exhibit prominent emission lines in their optical spectra. In the gamma-ray regime, their emission is predominantly due to IC. These sources are considered accretion-driven and extremely powerful across the spectrum, displaying the typical flat spectrum in the radio.

The link between these two classes has been highly debated within the framework of the Unified Model. It has been suggested that FSRQ could evolve into BL-Lac as it loses its power, leaving a rotationally driven structure (Cavaliere & D’Elia 2002). Traditionally, all blazars were thought to be characterized by a flat radio spectrum. However, some studies addressing the issue with multi-wavelength data, e.g. (Massardi et al. 2016), have already highlighted that the situation may have varying nuances. Massardi et al. (2016) shows that about 90 % of the blazars in their sample have a remarkably smooth spectrum, well described by a power-law over the full range, suggesting that what dominates in the range from 5 to 150 GHz is a single emitting region, rather than the superposition of different compact regions self-absorbed up to different frequencies. Giroletti et al. (2016) as well draws a scenario that differs from the traditional view, combining MWA Commissioning Survey (MWACS, Hurley-Walker et al. 2014) observations at 180 MHz and gamma-ray emission. They show that extended steep spectrum emission might still be present in quasars at low frequencies, confirming the possible presence of a jet.

Nevertheless, to further explore the correlation between radio and gamma emission, deep and high-resolution radio panchromatic coverage is needed. The advent of wide-area, low-frequency surveys, such as GaLactic and Extragalactic All-sky Murchison Widefield Array eXtended (GLEAM-X, Hurley-Walker et al. 2022) and the ASKAP surveys, have extended the radio coverage of the southern sky to lower frequencies. In particular, the FLASH continuum survey, opens a new window for detailed studies of synchrotron emission and its connection to gamma-ray sources. These data offer an unexplored perspective to the low energy emission of blazars.

In this work, we investigate the radio emission of 4FGL blazars detected in the FLASH continuum survey (Yoon et al. 2024), reconstructing their spectral energy distributions (SEDs) using multi-frequency radio data from FLASH, Rapid ASKAP Continuum Survey (RACS, McConnell et al. 2020; Hale et al. 2021), GLEAM-X (Hurley-Walker et al. 2022), the Australian Telescope compact array 20 GHz (AT20G, Murphy et al. 2010) survey, and the Atacama Large Millimeter Array CALibrators catalogue (ALMACAL, Oteo et al. 2016). We analyse their spectral trends, explore the presence of re-triggered spectral features, and study correlations with gamma-ray and X-ray emissions. Our findings provide new insights into blazar jet properties, their evolutionary states, and their role as cosmological tracers of neutral gas distribution. These results play a fundamental role in projects like FLASH, which leverage the characteristics

of blazars to study HI absorption, neutral gas evolution, and jet-environment interactions. This study also lays the groundwork for future investigations with the SKA Observatory (SKAO) and the Cherenkov Telescope Array (CTA), extending blazar studies into the next-generation radio and gamma-ray era.

## 2. Sample selection

**Table 1.** This table lists the surveys used in this study, showing how many counterparts we found and the spectral window covered. 4FGL is the starting point of this selection, counting 3419 blazars candidates.

Survey	# Matches	Spectral coverage
4FGL	-	100 MeV-1 TeV
eROSITA	65	0.2-10 keV
QUAIA	77	380-1080 nm
SDSS	30	u,g,r,i,z
ALMACAL	21	95-350 GHz
AT20G	32	4, 8, 20 GHz
RACS	165	887.5-2367.5 MHz
FLASH	165	711.5-999.5 MHz
GLEAM-X	97	72-231 MHz

The starting point for our sample selection was the 4FGL catalogue, DR4 (Ballet et al. 2023). Our sample consists of the BL-Lac (BLLs), FSRQs and Blazar Candidates of Uncertain type (BCUs) from this catalogue with counterparts in the FLASH continuum maps. In particular, we have used the 50 FLASH maps flagged as good, which were downloaded up to November 21, 2024 (Figure 1). Since the survey is still ongoing, the number of publicly available good fields may have increased since then. In this section, we will outline the primary catalogues used and detail the criteria for selecting the sources for our sample. The surveys used in this works are summarised in Table 1.

### 2.1. FLASH

FLASH is a radio survey conducted with the ASKAP. FLASH is designed to detect neutral hydrogen in absorption against bright radio continuum sources, probing the diffuse and dense phases of the intergalactic and interstellar medium over cosmological scales. The survey covers a redshift range of  $0.4 < z < 1.0$ . In this work, we make use of the FLASH continuum observations. FLASH continuum observations cover the frequency range 711.5–999.5 MHz, with a typical sensitivity of  $\sim 0.2$  mJy/beam and an angular resolution of  $\sim 15''$ .

### 2.2. 4FGL

The 4FGL represents the most comprehensive survey in the 100 MeV–1 TeV energy range. It is based on eight years of *Fermi* mission data, and includes over 5000 sources. Each source is characterized by its position, gamma-ray flux (including photon flux, energy flux, flux in different energy bands, and temporal variability across 96 monthly time bins), and spectral properties such as the photon index. The typical 95% positional confidence radius is approximately  $\sim 0.05$ – $0.1$  deg, depending on the source’s brightness and location in the sky (Ballet et al. 2023).

### 2.3. Selection process

We performed a cross-match between the two catalogues, using a radius of 0.1 deg, corresponding to the Full Width at Half

**Table 2.** Summary of the median radio properties of the 59 fitted sources from RadioSED.

Quantity	Median Value
$\alpha_{\text{retrig}}$	-0.5
$\alpha_{\text{thick}}$	0.2
$\alpha_{\text{thin}}$	-0.6
$\nu_{\text{peak-rest}}$	4.6 GHz
$\nu_{\text{trough-rest}}$	1.0 GHz

Maximum (FWHM) of LAT, as, between the two instruments, it possesses the least effective angular separation since ASKAP beam size is of  $\sim 15$  arcsec at 855 MHz (FLASH central frequency). Given the huge difference in the resolving power of the surveys, we visually inspected the data to exclude spurious and ambiguous pairings (Figure 2):

- As FLASH is composed of isolated mosaics (Figure 1), some of the sources happened to be on the edge of the fields, where the reliability drops down;
- In some cases, more than one source was equally probable to be the counterpart.

In the second case, we did not directly exclude the sources. Instead, we took advantage of other existing radio surveys, namely AT20G (Murphy et al. 2010; Massardi et al. 2011), RACS (McConnell et al. 2020), and GLEAM-X (Hurley-Walker et al. 2022), to decide, via visual inspection, which FLASH source was the most suitable counterpart. Nevertheless, for some objects it was impossible to determine which was the more likely counterpart, and, thus, we classified them as UNCERTAIN. We got a total of 259 cross-matched sources, 165 of which are classified as IN, 33 as OUT, and 80 as UNCERTAIN.

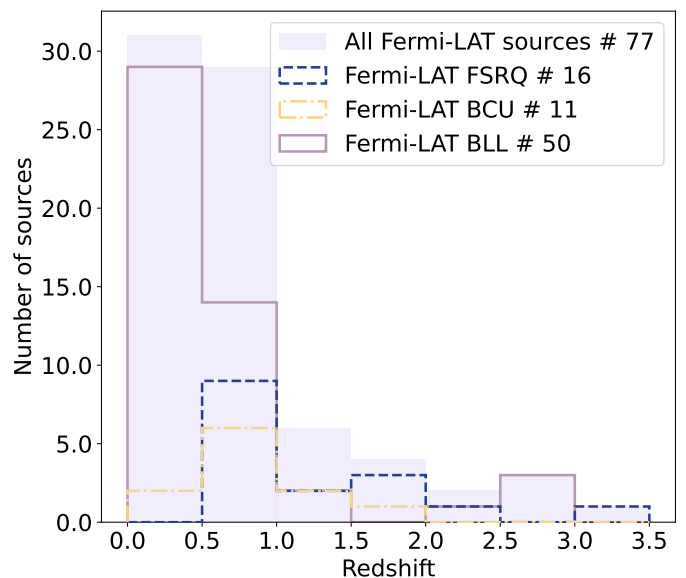
#### 2.4. The spectroscopic sub-sample

To find the sources' spectroscopic redshifts, we cross-matched the FLASH positions of the sources in our sample with the Sloan Digital Sky Survey (SDSS) DR17 survey and the Gaia-unWISE Quasar Catalog (QUAIA), using a radius of 5 arcsec. The SDSS covers  $\sim 14000$  deg<sup>2</sup> of the sky with a typical photometric sensitivity of 22.5 magnitudes in five optical bands (u, g, r, i, z) and a spatial resolution of  $\sim 1.4$  arcsec, providing spectra of the objects with a resolution of  $R \sim 2000$  at 3600–10400 Å. The SDSS overlaps FLASH in the equatorial area. QUAIA is an all-sky spectroscopic quasar sample. The catalogue draws on the 6,649,162 quasar candidates identified by the Gaia mission that have redshift estimates from the space observatory's low-resolution blue photometer/red photometer spectra. As a result, we achieved a total of 77 spectroscopically confirmed objects. The median redshift of these sources is 0.77, consistent with the overall FLASH catalogue (3). Figure 3 illustrates that BL-Lacs are generally at lower redshifts than FSRQs, bolstering the hypothesis of a parent-child relationship between the two populations. However, a larger spectroscopic sample is required to assess this scenario.

### 3. Methods

#### 3.1. Radio properties

To fully reconstruct the radio spectral energy distribution of the sources and, thus, retrieve their properties, we used all the radio data available for the objects in our sample.

**Fig. 3.** The distribution of spectroscopic redshifts from SDSS for sources marked as "IN" with a spectroscopic counterpart.

A key aspect to consider when analyzing multi-frequency data is the significant disparity in angular resolution across different surveys. At lower frequencies (e.g., GLEAM-X at  $\sim 72$ –231 MHz), the resolution is  $\sim 45''$ , while at 20 GHz (AT20G) it improves to a few arcseconds. This resolution mismatch could introduce uncertainties when associating extended radio structures with gamma-ray sources. However, since most blazars are expected to be compact at GHz frequencies, this effect is likely minimal.

We cross-matched the FLASH coordinates from our catalogue with GLEAM-X, RACS, AT20G, and ALMACAL (Oteo et al. 2016), enabling us to achieve comprehensive photometric coverage across radio frequencies, ranging from 72 MHz (GLEAM-X) to approximately 30 GHz (ALMACAL). This section will outline the development of the radio multi-wavelength catalogue, detail the SED-fitting process, and present the results derived from this procedure.

RACS covers the whole sky at  $-90 < \delta < 49$  at  $\sim 887.5/943.5$  (RACS-low, McConnell et al. 2020; Hale et al. 2021), 1367.5 (RACS-mid, Duchesne et al. 2023) and 1655.5 MHz (RACS-high, Duchesne et al. 2025), reaching a sensitivity of  $\sim 0.25$  (RACS-low) and 0.2 mJy/beam (RACS-mid, high) with a resolution of  $\sim 15''$  (RACS-low),  $10''$  (RACS-mid) and  $8''$  (RACS-high). Thus, RACS-low observations enable us to explore the sub-GHz emission as well. We cross-matched the catalogue using a  $15''$  radius and, as expected, we found that all of our sources have a counterpart in RACS.

GLEAM-X covers an area of 1447 deg<sup>2</sup> around the South Galactic Pole region covering  $-32.7 < \delta < -20.7$  with a median sensitivity 6.35 mJy/beam and a median resolution of  $45''$  (Hurley-Walker et al. 2022). The main advantage of the GLEAM-X survey is that it is composed of twenty frequency bands in the range 72–231 MHz. This interval samples the MHz side of the radio SED, where self-absorption processes occur. The SED fitting procedure, described in the following subsection, included all the sources with at least 5 photometric detections in the radio bands.

### 3.2. Radio SED-fitting

We performed the SED-fitting using RADIOSED (Kerrison et al. 2024), a software designed to model and fit radio SEDs of astrophysical sources (Figure 4, Appendix A). This tool is particularly suited for analysing multi-frequency radio data, allowing us to disentangle the contributions of various emission mechanisms by testing multiple spectral models.

#### 3.2.1. SED-fitting and model selection

RADIOSED supports different functional forms to describe radio SEDs. Throughout this paper, we classify the spectral shapes as follows, consistently with Kerrison et al. (2024):

- **Power Law:** A simple model given by

$$S_\nu \propto \nu^\alpha, \quad (1)$$

where  $\alpha$  is the spectral index. Flat spectrum sources, traditionally associated with blazar jets (Massaro et al. 2013a,b), fall into this category.

- **Peaked Spectrum:** Sources exhibiting a turnover in their SED, where the flux density increases up to a peak frequency  $\nu_{\text{peak}}$  and then decreases. This behaviour can indicate synchrotron self-absorption or a young radio source. We model these sources using the functional form (Snellen et al. 1998; Callingham et al. 2017; Slob et al. 2022):

$$S_\nu = \frac{S_p}{1 - e^{-1}} \left( 1 - e^{-(\nu/\nu_p)^{\alpha_{\text{thin}} - \alpha_{\text{thick}}}} \right) \left( \frac{\nu}{\nu_p} \right)^{\alpha_{\text{thick}}}, \quad (2)$$

where  $S_p$  is the flux density at  $\nu_p$ , and  $\alpha_{\text{thin}}$  and  $\alpha_{\text{thick}}$  are the spectral indices for the optically thin and thick components.

- **Curved Peaked Spectrum:** A modification of the peaked spectrum including a curvature term (Orienti et al. 2007, 2010):

$$\log S_\nu = a + \log \nu (b + c \log \nu), \quad (3)$$

where  $c$  is the curvature parameter.

- **Re-triggered Peaked Spectrum:** A peaked SED with a secondary low-frequency upturn, suggesting episodic jet activity or restarted accretion (Edwards & Tingay 2004). It is modeled as:

$$S_\nu = \frac{S_p}{1 - e^{-1}} \left[ 1 - e^{-(\nu/\nu_p)^{\alpha_{\text{thin}} - \alpha_{\text{thick}}}} \right] \left( \frac{\nu}{\nu_p} \right)^{\alpha_{\text{thick}}} + S_0 \nu^\alpha. \quad (4)$$

Each model is fitted independently, and the best-fit model is determined through Bayesian model selection. RADIOSED computes the Bayes factor to compare the likelihoods of different models, selecting the one with the highest posterior probability.

We adopt non-informative priors (log-uniform/linear-uniform) as described in Table 2 of Kerrison et al. (2024), to ensure a statistically robust classification of spectral types, providing a reliable characterization of the blazar SEDs in our sample.

However, the SED modeling does not account for intrinsic variability between epochs, which can affect the interpretation of blazar spectra. This represents a limitation of our modeling approach that should be considered when analyzing the results.

## 4. Results

### 4.1. Results from the SED-fitting

From the SED fitting of the radio emission, we retrieved the spectral behaviour of the sources, finding that most of them are well described by the Re-triggered Peaked Spectrum, as defined by Equation 4. This smooth behaviour, in contrast to a flat spectrum, suggests that the emission is dominated by a single emitting region rather than by the superposition of multiple compact, self-absorbed regions, as indicated by the classic blazar paradigm (Massardi et al. 2016).

The main parameters retrieved from the SED-fitting (Table 2, Figure 4) are:

- $\nu_{\text{trough}}$ : the frequency corresponding to the minimum of the SED. After this point, if present, the SED starts rising.
- $\alpha_{\text{trough}}$ : the spectral index at frequencies  $\nu < \nu_{\text{trough}}$ , usually corresponding to GLEAM-X photometric points for our sample.
- $\nu_{\text{peak}}$ : the frequency where, if present, the peak of the SED takes place.
- $\alpha_{\text{thick}}$ : the spectral index at frequencies  $\nu_{\text{trough}} < \nu < \nu_{\text{peak}}$ , corresponding to the thick part of the peaked component.
- $\alpha_{\text{thin}}$ : the spectral index at frequencies  $\nu > \nu_{\text{peak}}$ , corresponding to the thin part of the peaked component.

Using the advanced surveys employed in this study, we conclude that at GLEAM-X wavelengths the spectral behaviour is not completely flat ( $\alpha \sim -0.5$ , Table 2). This finding opens the path to an additional extended, steep-spectrum emission, previously missed (Massaro et al. 2013a,b; Nori et al. 2014). GLEAM-X is, in fact, sensitive to diffuse, low-frequency emission likely from older radio lobes that are missed in higher-frequency surveys.

According to the theory that  $t_{\text{cool}} \propto 1/\sqrt{\nu_{\text{peak}}}$ , where  $\nu_{\text{peak}}$  serves as a proxy for evolutionary timescales, our sample reveals that younger objects tend to exhibit their spectral upturn at higher frequencies while maintaining a low-frequency spectral index of  $\sim -0.5$  (Figure 5). Conversely, older sources are less constrained to a specific spectral index, but they all exhibit a spectral shape change around  $\sim 100$  MHz. This behaviour might indicate that a more powerful core might still be prominent and efficient in younger sources, efficiently refurbishing the jet with energetic electrons.

For most of the sources, the SED extends smoothly towards higher frequencies with a peaked spectrum emission, where it is possible to distinguish a thick part ( $\alpha_{\text{thick}}$ ) and a thin part ( $\alpha_{\text{thin}}$ ).

The median  $\nu_{\text{peakrest}}$  is  $\sim 4.6$  GHz and no hint of breaks due to ageing is present at high frequency.

In the radio colour-colour diagram, displayed in Figure 6, it emerges that most of the objects ( $\sim 57.6\%$ ) are in the fourth quadrant, i.e. have a hint of a peaked spectrum and  $\sim 10.2\%$  have a flat spectrum, after  $\nu_{\text{trough}}$ . This is a rather small percentage, indicating that in the GHz domain as well we would expect a single emitting region, rather than the superposition of a number of compact regions of different sizes, self-absorbed at different frequencies.

This single component dominating at  $\nu > \nu_{\text{trough}}$  could represent the compact self-absorbed segment that was re-activated at a later time. Meanwhile, the low-energy segment of the SED could delineate an extended remnant from earlier activity (Figure 7). Our results suggest that resolution differences have a limited impact on the main trends observed in the radio SEDs, as most sources are unresolved at GHz frequencies. However, deeper, high-resolution low-frequency surveys (e.g., LOFAR,

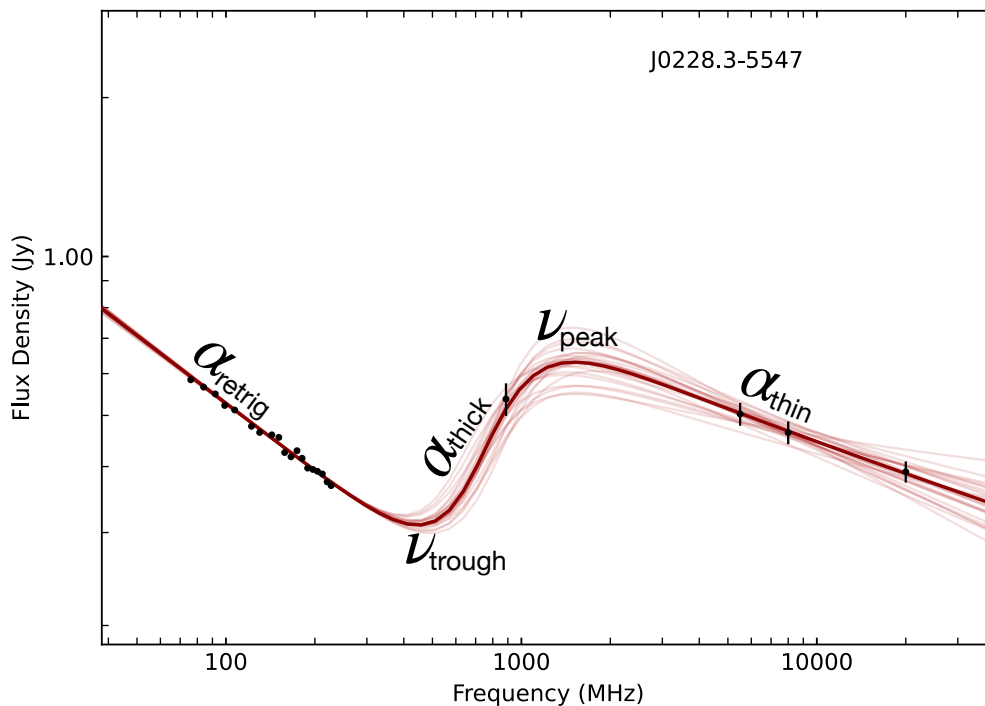


**Fig. 4.** Spectral Energy Distribution (SED) fitting for one of the selected blazars in our sample. The models incorporate GLEAM-X, RACS, AT20G, and ALMACAL data. The best-fit model is shown as a solid line, while individual photometric points are marked.

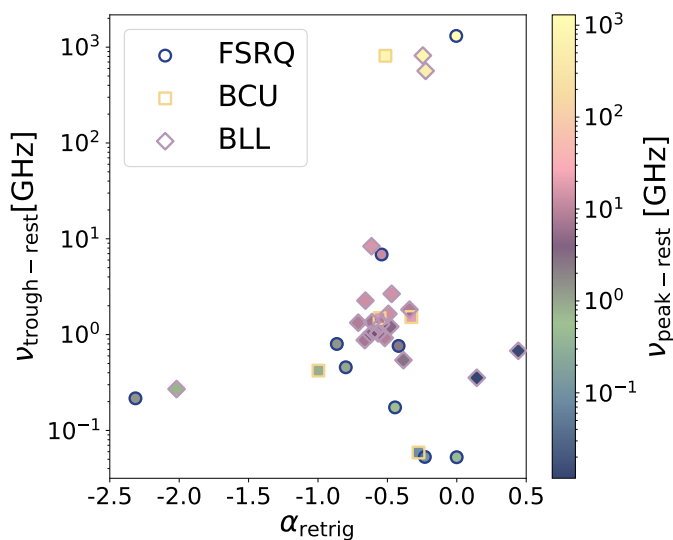


**Fig. 5.** Relation between the trough frequency  $\nu_{\text{trough}}$  and the spectral index at lower frequencies  $\alpha_{\text{trough}}$ . The colour scale represents the peak frequency  $\nu_{\text{peak}}$ , which can be used as a proxy for the cooling time of the source. The colours of the markers' edges represent the three blazar populations: FSRQ, BL-Lac and BCU.

SKA-Low) will be valuable for disentangling diffuse extended emission from compact jet components.

On the radio colour-colour diagram, BL-Lacs display a wide range of behaviours, whereas FSRQs tend to cluster in the flat region. This indicates that FSRQs undergo highly efficient electron pumping, which significantly boosts high-energy radio synchrotron emissions.

Conversely, both populations seem indistinguishable when considering  $\nu_{\text{trough}}$  and  $\alpha_{\text{trough}}$  (Figure 6) This may suggest that

**Table 3.** Median and correlation between the ratio of radio and X-ray luminosities for different object classes (All, FSRQ, BL-Lac). The values are expressed as a function of the luminosities at 150 MHz, 855 MHz, and 20 GHz, relative to the  $\gamma$ -ray luminosity.

		All	FSRQ	BL-Lac
$\log\left(\frac{L_{150\text{MHz}}}{L_\gamma}\right)$	Median	-3.07	-2.82	-3.25
	Correlation	0.70	0.77	0.93
$\log\left(\frac{L_{855\text{MHz}}}{L_\gamma}\right)$	Median	0.34	0.38	-0.48
	Correlation	0.70	0.92	0.85
$\log\left(\frac{L_{20\text{GHz}}}{L_\gamma}\right)$	Median	0.06	0.15	-0.14
	Correlation	0.78	0.20	0.98

the extremely low radio frequency emissions are remnants of the source's history, remaining unchanged by subsequent activities detected at higher frequencies, as the former emissions are confined to the outskirts, while the latter is linked to the nuclear core region.

## 5. Discussion

### 5.1. The Radio-gamma correlation

Using the redshift estimates, we have drawn a picture of the energy budget spent by the sources in the radio bands from  $\sim 72$  MHz to  $\sim 30$  GHz and in the *Fermi*-LAT bands. This, combined with the radio SED-fitting described in Section 4.1, allowed us to find the primary emitting components of the object and its evolutionary stage. The median value of the radio luminosity at 855 MHz is  $2.5 \times 10^{26} \text{WHz}^{-1}$  for the spectroscopic sample, with 25% of them having a luminosity  $> 1.8 \times 10^{27} \text{WHz}^{-1}$ . 25% of the sources have a  $\gamma$ -ray luminosity higher than  $> 1.8 \times 10^{27} \text{WHz}^{-1}$  and the median value is  $4.3 \times 10^{26} \text{WHz}^{-1}$ .

The correlation between radio and  $\gamma$ -ray emission, if present, supports the idea that they are both dominated by the relativistic

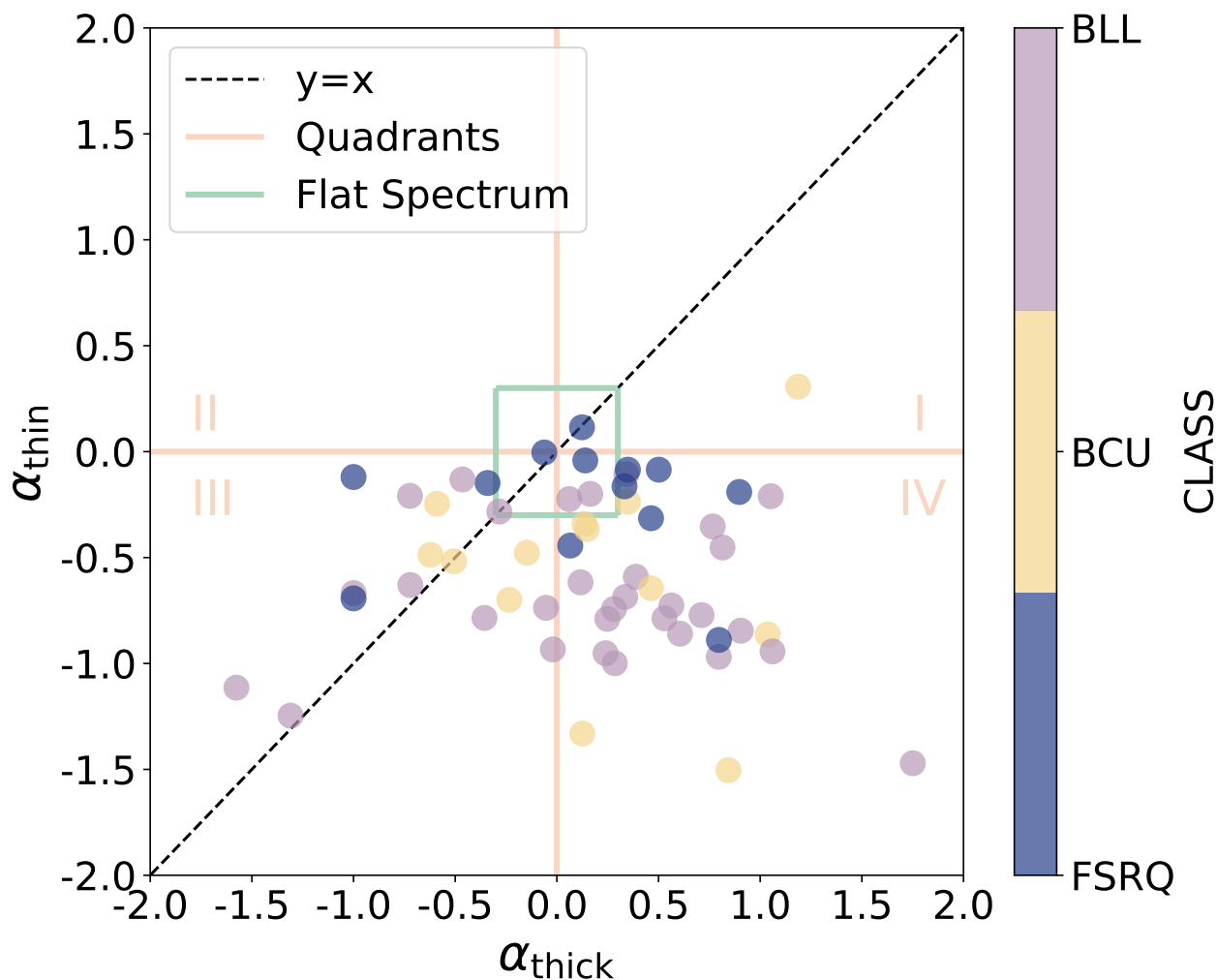


**Fig. 6.** Radio colour-colour diagram of the blazars in our sample, based on the spectral indices retrieved from the SED fitting. The colours represent the three blazar populations: FSRQ, BL-Lac and BCU.

jet (Giroletti et al. 2016; Mahony et al. 2016). In this work, we can observe how this relation behaves in different radio bands (Figure 8, Table 3). This is particularly useful, since the dominant emitting component varies along the radio spectrum, as we found through the SED-fitting. The luminosity at 855 MHz is closely tied to the  $\gamma$ -ray luminosity, indicating that, at this frequency, the jet significantly impacts both radio and gamma energy emissions, with a tight relation (correlation coefficient  $\rho \sim 0.70$ , see Figure 8). This suggests that at 885 MHz, we primarily observe the most powerful segment of the jet, nearest to the nucleus (Figure 7), potentially representing the re-activated section. This is supported by the way the radio- $\gamma$ -ray relation appears at 20GHz. Consequently, at high radio frequencies, the radio emission is overwhelmingly driven by a strong jet.

In Figure 8 the correlation between 150 MHz and  $\gamma$  emission is displayed. Although in this case as well there is a correlation between high and low energy emissions (correlation coefficient  $\sim 0.70$ ), there is an evident offset. A potential explanation might be that the extended synchrotron emission, which is not efficient enough at generating  $\gamma$ -rays, dominates this part of the spectrum. This scenario is in full agreement with the results obtained from the SED-fitting (Section 4.1).

The FSRQs dominate the bright end of the luminosity in both radio and  $\gamma$  and the e Radio-Gamma Correlation keeps holding

for both FSRQs and BL-Lacs. Nevertheless, as shown in Table 3, the radio- $\gamma$  correlation assumes higher values for FSRQs both at 150 and 855 MHz, approaching the point in which the radio and  $\gamma$  emission are perfectly balanced at lower frequencies. Thus, the FSRQs could saturate the relation already at lower frequencies. This suggests that FSRQs might generally exhibit more effective high-energy pumping across various scales and reflects the presence of a flat spectrum at  $\nu > \nu_{\text{trough}}$ , i.e. the emitting mechanism at 885 and 20 GHz is almost the same.

## 5.2. The Radio-X-ray correlation

To further explore the nature of blazars, we cross-matched our sample with the eROSITA all-sky survey (Merloni et al. 2024). 48 of the sources in the spectroscopic sample have an eROSITA counterpart within  $10''$ . The eROSITA telescope array aboard the Spektrum Roentgen Gamma (SRG) satellite began surveying the sky at 0.2-10 keV. The eROSITA DR1 covers  $\sim 14056 \text{ deg}^2$  with a median sensitivity in the 0.2-2 keV of  $\sim 10^{-14} \text{ erg cm}^{-2} \text{ s}^{-1}$ . For the cross-matched sources, we were able to study the relationship between X-ray and radio emission. We considered the energy range 0.2 - 2.0 keV for the X-ray luminosity.

Within this spectrum, the sources being analysed exhibit a median luminosity of  $6.9 \times 10^{20} \text{ WHz}^{-1}$ , with 25% of these

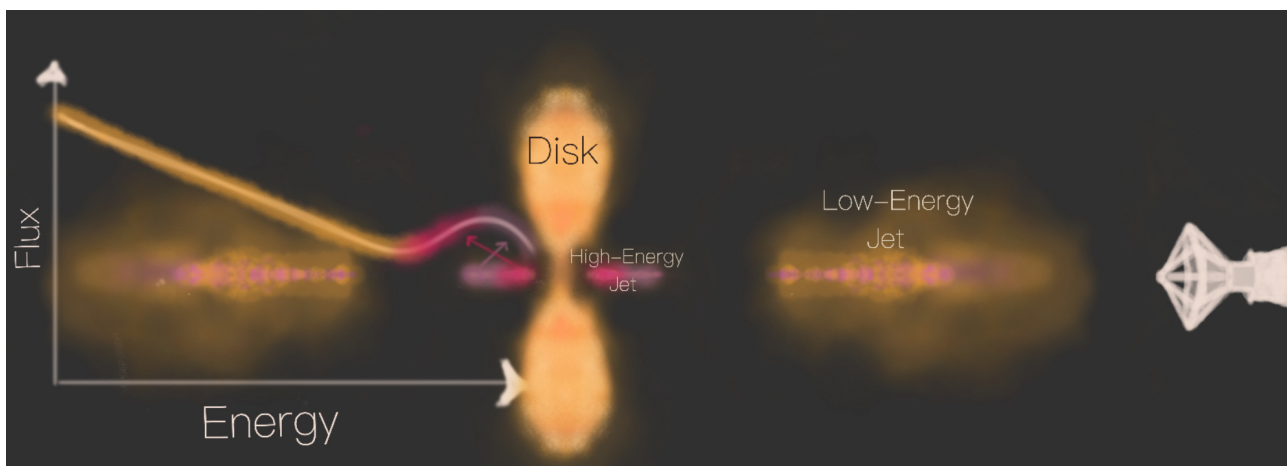


**Fig. 7.** Schematic representation of the physical interpretation of blazar radio emission outlined in this paper. The figure illustrates the interplay between compact self-absorbed components and extended steep-spectrum emission, which may indicate episodic jet activity or restarted AGN cycles.

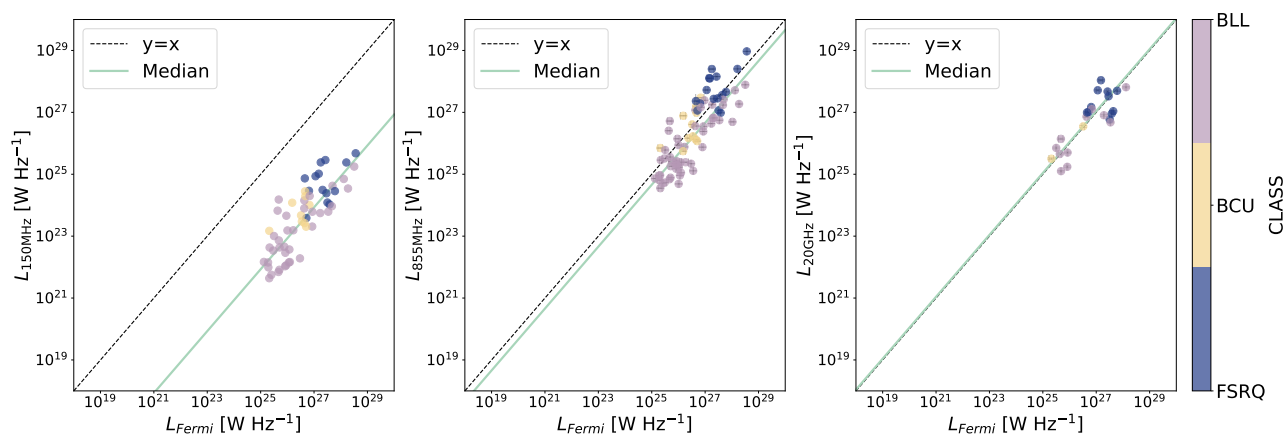


**Fig. 8.** Radio luminosity at 150 MHz (*left*), 855 MHz (*centre*) and 20 GHz (*right*) as a function of the  $\gamma$ -ray luminosity from *Fermi*-LAT. The black dashed line and the green line indicate the bisector and the median trend, respectively. The colours indicate the blazar class from the 4FGL catalogue.

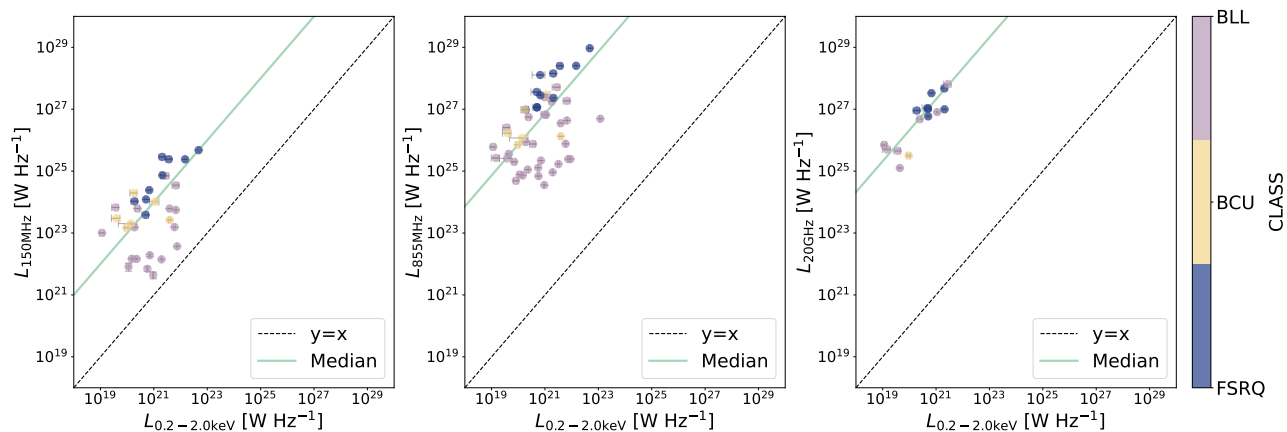


**Fig. 9.** Radio luminosity at 150 MHz (*left*), 855 MHz (*centre*) and 20 GHz (*right*) as a function of the X-ray luminosity from *eROSITA*. The black dashed line indicates the bisector. The colours indicate the blazar class from the 4FGL catalogue.

sources having a luminosity exceeding  $2.8 \times 10^{21} \text{ W Hz}^{-1}$ . The main driver of the emission in this range is the hot corona, which closely traces the accretion disk, especially in FSRQs. The Radio-X-ray correlation is shown in Figure 9. We show the results in Table 4 and we found almost no correlation for the 855

MHz, but a tight one at 150 MHz. In this particular situation, even giving just a glance at Figure 9, it is clear that the global behaviour might be misleading and not truly representative of the physical processes taking place. It is only distinguishing the different classes of blazars that the real picture pops out, as the

**Table 4.** Median and correlation between the ratio of radio and X-ray luminosities for different object classes (All, FSRQ, BL-Lac). The values are expressed as a function of the luminosities at 150 MHz, 855 MHz, and 20 GHz, relative to the X-ray luminosity in the 0.2–2.0 keV range.

		All	FSRQ	BL-Lac
$\log\left(\frac{L_{150\text{MHz}}}{L_{0.2-2.0\text{keV}}}\right)$	Median	3.00	3.55	2.09
	Correlation	0.80	0.81	0.28
$\log\left(\frac{L_{855\text{MHz}}}{L_{0.2-2.0\text{keV}}}\right)$	Median	5.86	6.62	6.62
	Correlation	0.32	0.97	0.02
$\log\left(\frac{L_{20\text{GHz}}}{L_{0.2-2.0\text{keV}}}\right)$	Median	6.32	6.34	6.33
	Correlation	0.82	0.48	0.99

degree of correlation is clearly unbalanced between FSRQs and BL-Lacs, indicating that the radio and soft X-ray emissions are tightly correlated for FSRQs, whereas in BL-Lacs, the relationship is highly scattered.

The results obtained (4) confirm that FSRQs are in an accretion-driven regime, which fuels both the radio jet and the disk emission. On the other hand, in BL-Lacs the jets are mainly rotation-driven. However, alternative factors could contribute to the observed trends. For instance, BL-Lacs exhibit higher variability in the X-ray band, which may introduce additional scatter in the correlation (Ghisellini et al. 2017).

Moreover, the impact of the circumnuclear medium could play a role in shaping the X-ray emission properties, particularly in FSRQs, where disk-related processes contribute significantly to the total luminosity. A deeper understanding of these effects will require time-domain studies incorporating simultaneous X-ray and radio observations.

When comparing the X-ray luminosity with the 20 GHz emission, it is essential to account for selection bias. The sources in our sample that have both a 20 GHz and a X-ray counterpart represent a highly efficient subset of our data. Consequently, the tighter correlation between X-ray and radio emissions is not surprising, given that the fraction of FSRQs is higher at these frequencies compared to lower frequencies. Deeper millimeter observations are required to gain a comprehensive scientific understanding of the behaviour at higher frequencies.

## 6. Summary and future perspectives

### 6.1. Summary

This study explores the radio properties of 4FGL blazars detected in the FLASH continuum survey, focusing on their spectral characteristics and multi-wavelength correlations. The main findings are summarized as follows:

- **Radio SED Characteristics:** About 50% of the sources in the sample exhibit a clearly re-triggered peaked spectrum, while for approximately 14% of them, such a spectrum can be safely excluded. This suggests that the emission is dominated by a single emitting region rather than by the superposition of multiple compact, self-absorbed regions.
- **Spectral Trends:** The median peak frequency ( $\nu_{\text{peak}}$ ) is approximately 4.6 GHz, with 55% of sources showing peaks above 10 GHz (high-frequency peakers), indicating a population of likely young or recently re-activated blazars.
- **Extended Emission:** At low frequencies (e.g., below 100 MHz), the emission is characterised by a spectral index of  $\sim -0.54$ , consistent with the presence of an additional steep-spectrum emission, previously missed due to the lack of high-resolution and deep low frequency data.

- **Radio-gamma correlation:** A strong correlation between radio and gamma-ray luminosities was identified, particularly at 855 MHz, emphasizing the dominant contribution of relativistic jets to the observed multi-wavelength emission.
- **Radio-X-ray correlation:** The X-ray luminosity (0.2–2.0 keV) is tightly correlated with radio luminosity for FSRQs, reflecting their accretion-driven nature, while BL-Lacs show a more scattered relationship, consistent with their jet-driven dynamics.
- **Blazar Subclass Differences:** FSRQs display more efficient high-energy pumping and dominate the bright end of the radio and gamma luminosity spectrum, while BL-Lacs exhibit greater variability in spectral behavior, reflecting their evolutionary differences.

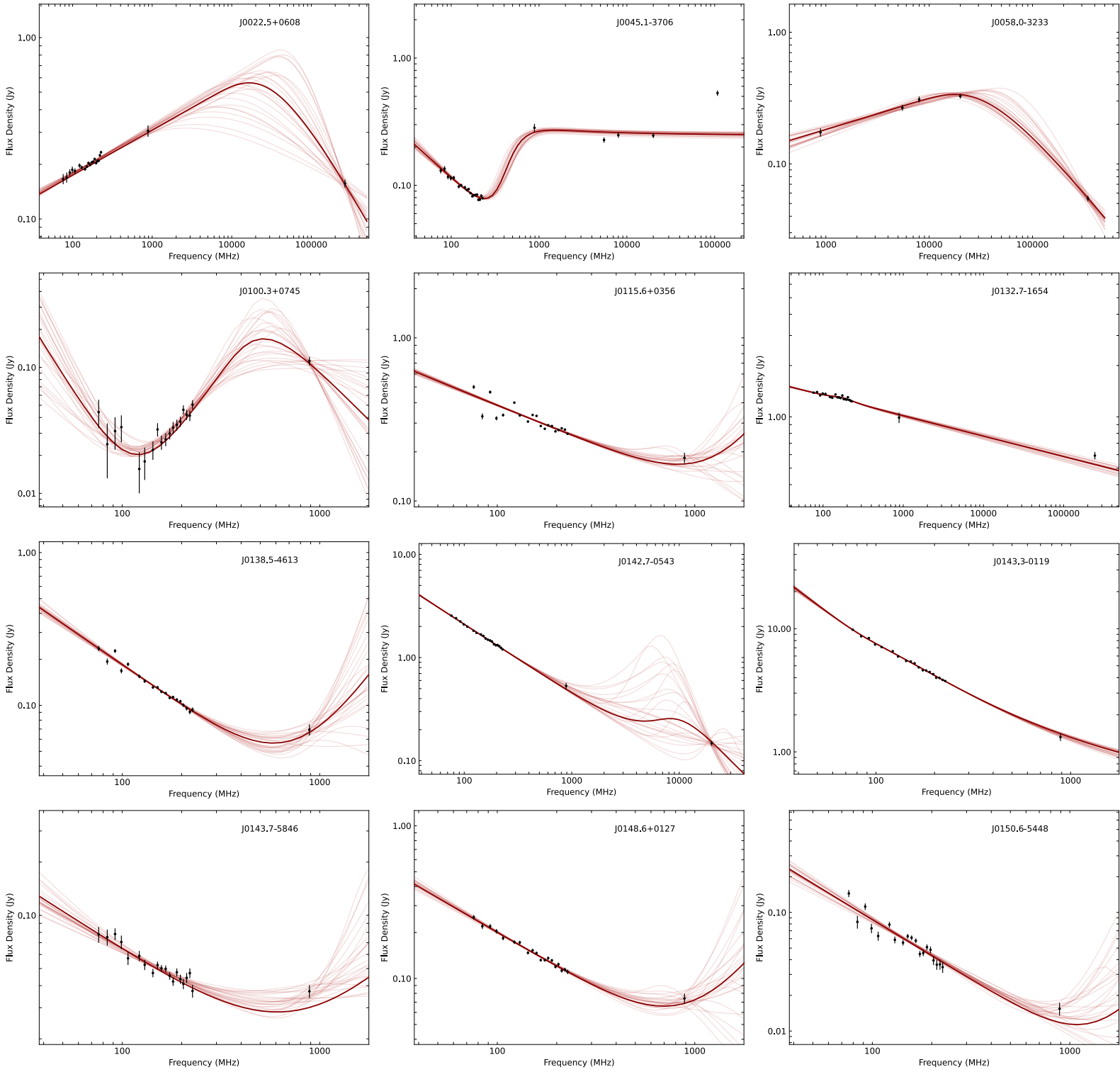
### 6.2. Future perspectives

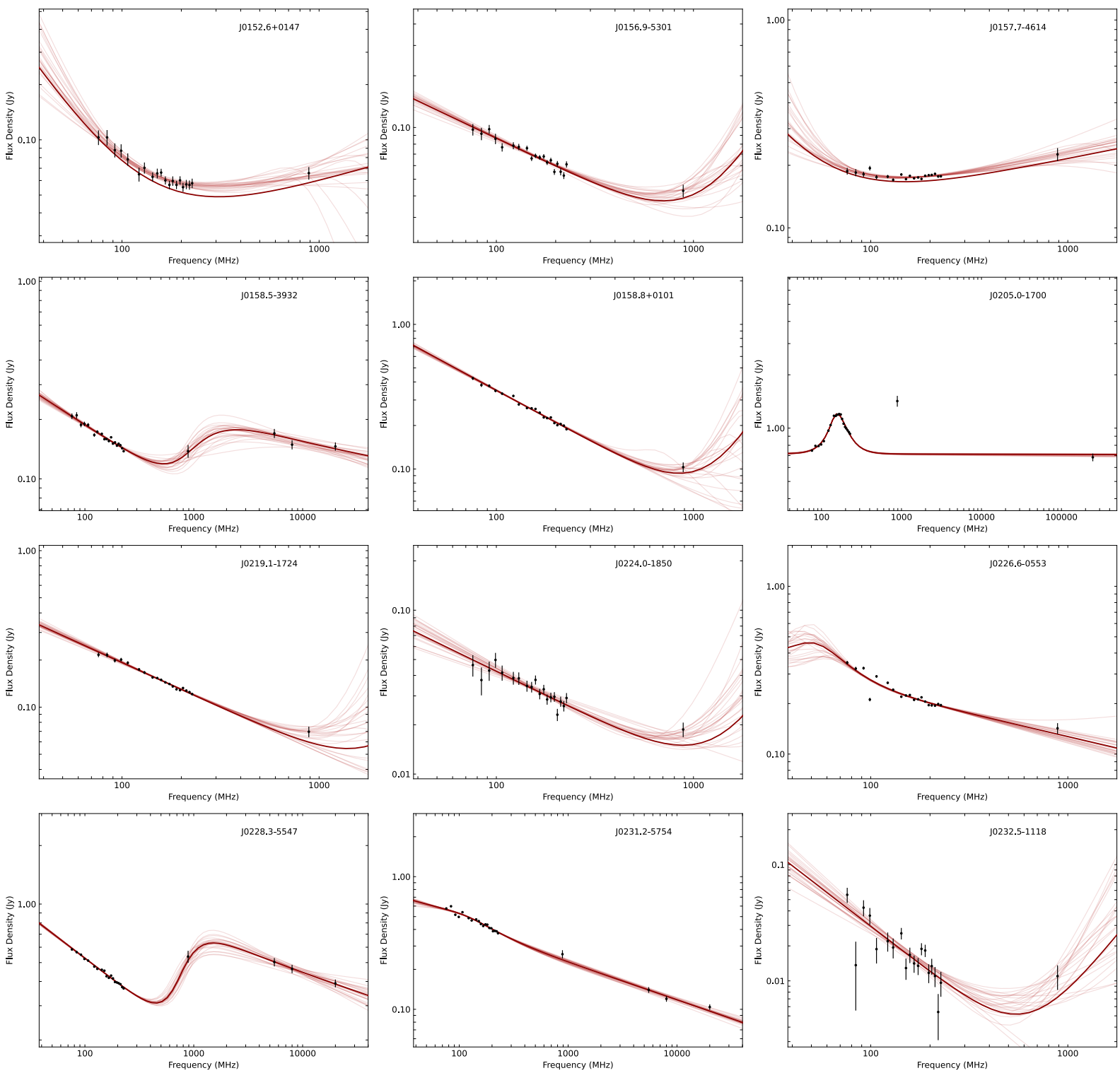
Building on these findings, future studies will aim to deepen our understanding of the physical and environmental properties of blazars. Firstly, FLASH is an ongoing survey; therefore, we will expand the blazar sample to include the full 5-year dataset upon completion. Further, a key next step will be to analyse the spectroscopic properties of these objects using FLASH, XMM-Newton, and optical lines data (e.g., broad-line region emission). This will help us provide detailed insights into the physics of blazars and their environments, offering clues about the retriggering mechanism and the dual nature of their radio emission. Finally, leveraging instruments like the SKAO and CTA will allow for broader frequency coverage and improved sensitivity, enabling the detection of faint sources and the study of synchrotron emission at unprecedented depth.

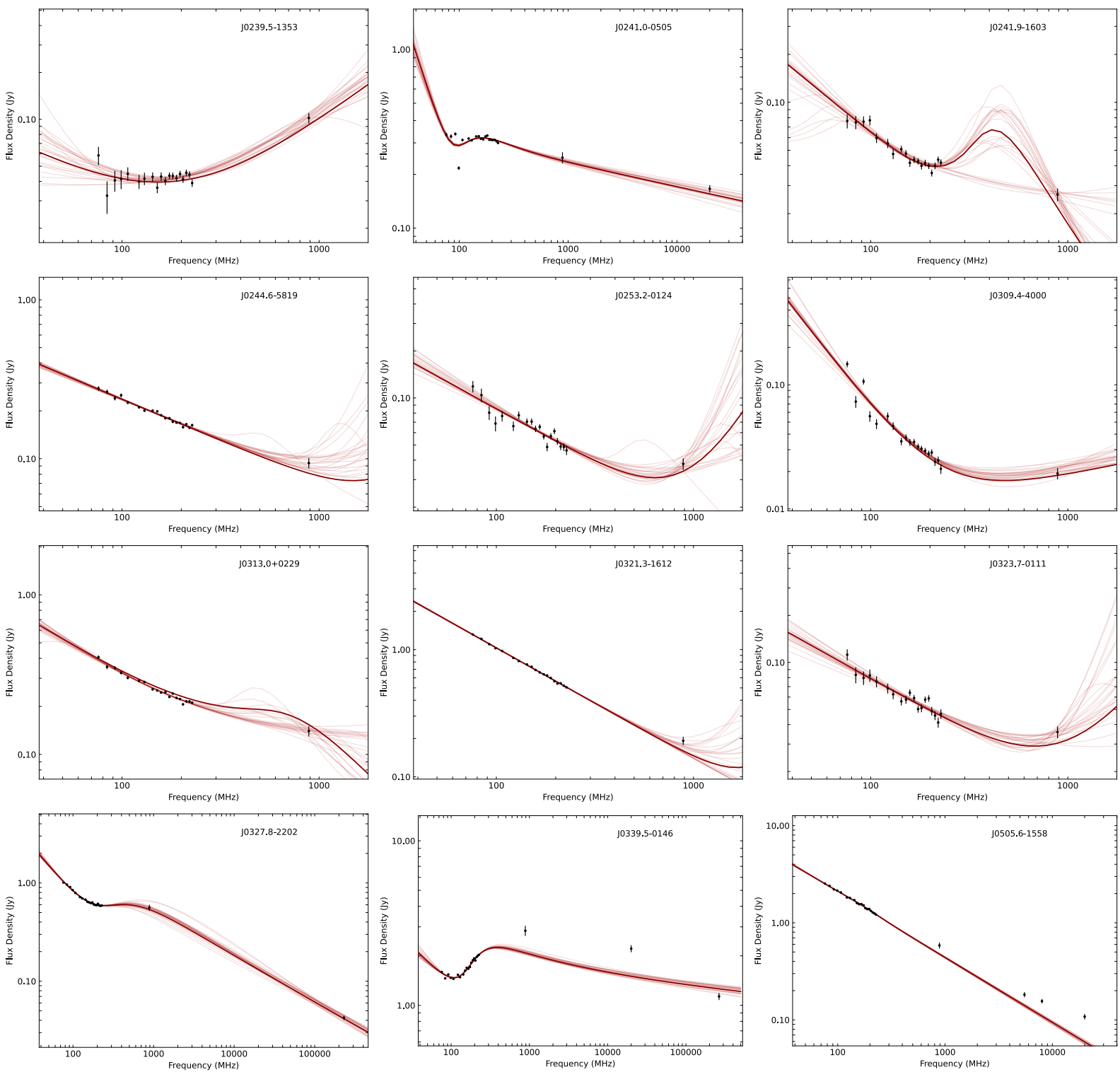
*Acknowledgements.* This work was carried out in part during an Erasmus+ exchange program at CSIRO ATNF in Marsfield, Sydney. MB gratefully acknowledges the support provided by Erasmus+ and the CSIRO ATNF for facilitating this research opportunity. This scientific work uses data obtained from Inyarrimanha Ilgari Bundara, the CSIRO Murchison Radio-astronomy Observatory. We acknowledge the Wajarri Yamaji People as the Traditional Owners and native title holders of the Observatory site. CSIRO's ASKAP radio telescope is part of the Australia Telescope National Facility (<https://ror.org/05qajvd42>). Operation of ASKAP is funded by the Australian Government with support from the National Collaborative Research Infrastructure Strategy. ASKAP uses the resources of the Pawsey Supercomputing Research Centre. Establishment of ASKAP, Inyarrimanha Ilgari Bundara, the CSIRO Murchison Radio-astronomy Observatory and the Pawsey Supercomputing Research Centre are initiatives of the Australian Government, with support from the Government of Western Australia and the Science and Industry Endowment Fund. This work was partially funded from the projects: INAF GO-GTO Normal 2023 funding scheme with the project "Serendipitous H-ATLAS-fields Observations of Radio Extragalactic Sources (SHORES)". MVZ acknowledges partial financial support from the "Fondazione CR Firenze" with the program "Ricercatori a Firenze 2023". The colour palettes used in this paper were directly extracted from Claude Monet's paintings *Water Lilies* and *San Giorgio Maggiore at Dusk*.

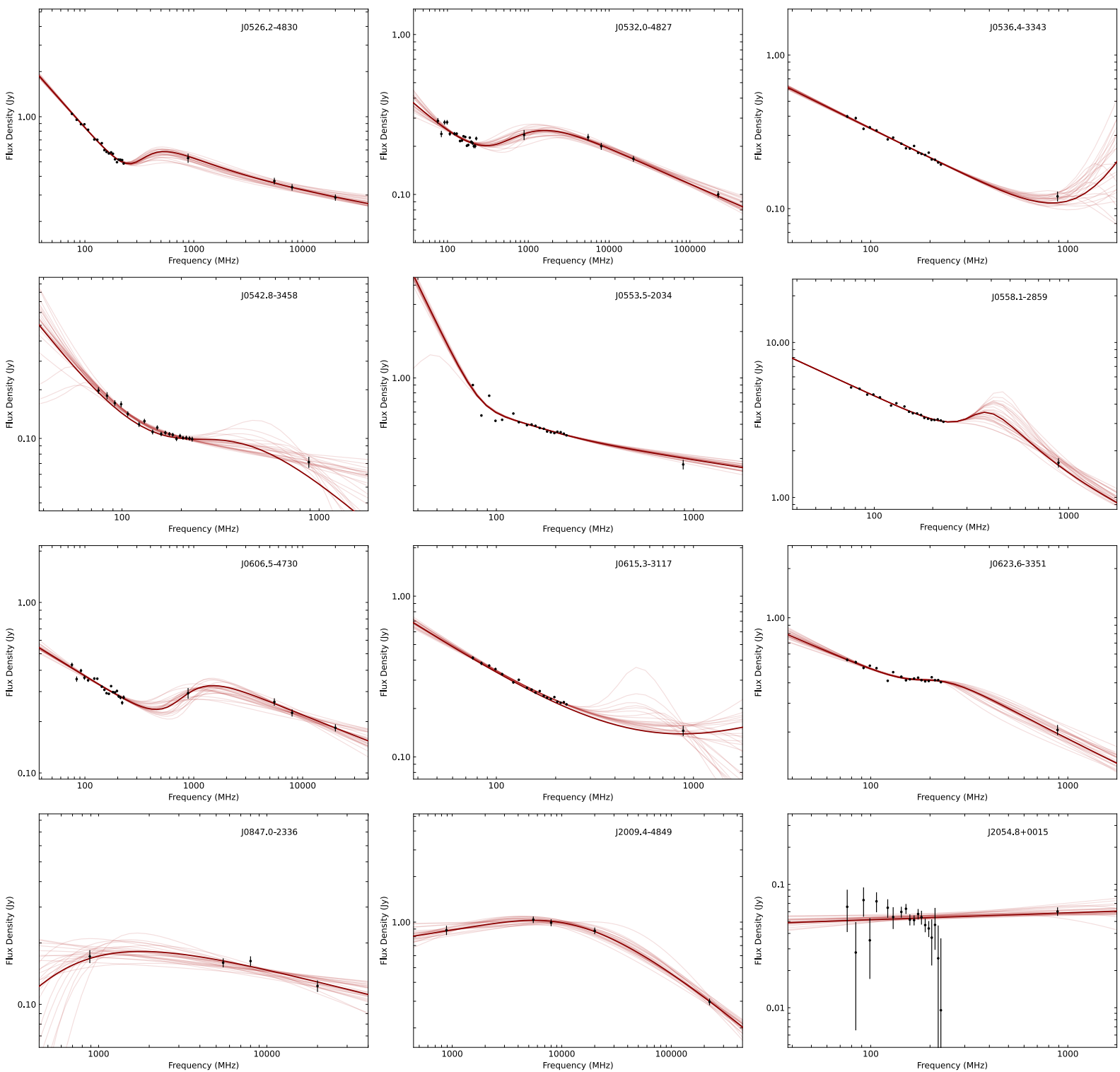
## Appendix A: Spectral Energy Distributions

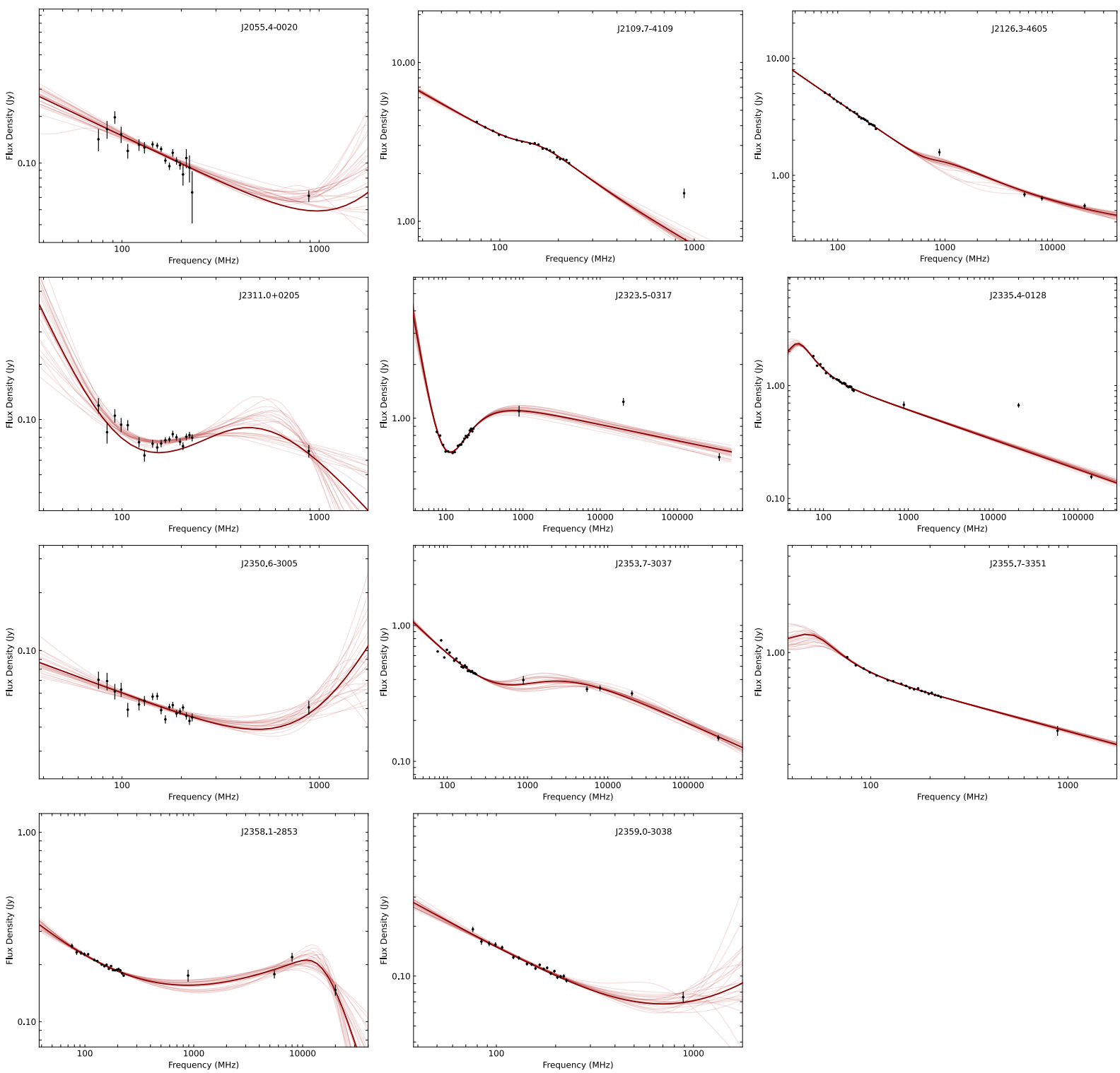
In this Appendix we show the fitted SEDs. The best-fit model is shown as a solid dark-red line.











## References

- Abdo, A. A., Ackermann, M., Ajello, M., et al. 2010, *ApJS*, 188, 405
- Acero, F., Ackermann, M., Ajello, M., et al. 2015, *ApJS*, 218, 23
- Ballet, J., Bruel, P., Burnett, T. H., Lott, B., & The Fermi-LAT collaboration. 2023, arXiv e-prints, arXiv:2307.12546
- Callingham, J. R., Ekers, R. D., Gaensler, B. M., et al. 2017, *ApJ*, 836, 174
- Cavaliere, A. & D'Elia, V. 2002, *ApJ*, 571, 226
- Duchesne, S. W., Ross, K., Thomson, A. J. M., et al. 2025, arXiv e-prints, arXiv:2501.04978
- Duchesne, S. W., Thomson, A. J. M., Pritchard, J., et al. 2023, *PASA*, 40, e034
- Edwards, P. G. & Tingay, S. J. 2004, *A&A*, 424, 91
- Ghisellini, G., Righi, C., Costamante, L., & Tavecchio, F. 2017, *MNRAS*, 469, 255
- Giroletti, M., Massaro, F., D'Abrusco, R., et al. 2016, *A&A*, 588, A141
- Hale, C. L., McConnell, D., Thomson, A. J. M., et al. 2021, *PASA*, 38, e058
- Hurley-Walker, N., Galvin, T. J., Duchesne, S. W., et al. 2022, *PASA*, 39, e035
- Hurley-Walker, N., Morgan, J., Wayth, R. B., et al. 2014, *PASA*, 31, e045
- Kerrison, E. F., Allison, J. R., Moss, V. A., Sadler, E. M., & Rees, G. A. 2024, *MNRAS*, 533, 4248
- Mahony, E. K., Morganti, R., Prandoni, I., et al. 2016, *MNRAS*, 463, 2997
- Maina, E. K., Mohapatra, A., Józsa, G. I. G., et al. 2022, *MNRAS*, 516, 2050
- Massardi, M., Bonaldi, A., Bonavera, L., et al. 2016, *MNRAS*, 455, 3249
- Massardi, M., Ekers, R. D., Murphy, T., et al. 2011, *MNRAS*, 412, 318
- Massaro, F., D'Abrusco, R., Giroletti, M., et al. 2013a, *ApJS*, 207, 4
- Massaro, F., Giroletti, M., Paggi, A., et al. 2013b, *ApJS*, 208, 15
- McConnell, D., Hale, C. L., Lenc, E., et al. 2020, *PASA*, 37, e048
- Merloni, A., Lamer, G., Liu, T., et al. 2024, *A&A*, 682, A34
- Murphy, T., Sadler, E. M., Ekers, R. D., et al. 2010, *MNRAS*, 402, 2403
- Nolan, P. L., Abdo, A. A., Ackermann, M., et al. 2012, *ApJS*, 199, 31
- Nori, M., Giroletti, M., Massaro, F., et al. 2014, *ApJS*, 212, 3
- Orienti, M., Dallacasa, D., & Stanghellini, C. 2007, *A&A*, 475, 813
- Orienti, M., Dallacasa, D., & Stanghellini, C. 2010, *MNRAS*, 408, 1075
- Oteo, I., Zwaan, M., Ivison, R., Smail, I., & Biggs, A. 2016, *The Messenger*, 164, 41
- Padovani, P. 2016, *A&A Rev.*, 24, 13
- Padovani, P., Boccardi, B., Falomo, R., & Giommi, P. 2022a, *MNRAS*, 511, 4697
- Padovani, P., Giommi, P., Falomo, R., et al. 2022b, *MNRAS*, 510, 2671
- Slob, M. M., Callingham, J. R., Röttgering, H. J. A., et al. 2022, *A&A*, 668, A186
- Snellen, I. A. G., Schilizzi, R. T., de Bruyn, A. G., et al. 1998, *A&AS*, 131, 435
- Srianand, R., Gupta, N., Petitjean, P., et al. 2022, *Monthly Notices of the Royal Astronomical Society*, 516, 1339
- Tavecchio, F. 2017, in *American Institute of Physics Conference Series*, Vol. 1792, 6th International Symposium on High Energy Gamma-Ray Astronomy (AIP), 020007
- Tingay, S. J., Goetze, R., Bowman, J. D., et al. 2013, *PASA*, 30, e007
- Urry, C. M. & Padovani, P. 1995, *PASP*, 107, 803
- Whiting, M. & Humphreys, B. 2012, *PASA*, 29, 371
- Yoon, H., Sadler, E. M., Mahony, E. K., et al. 2024, arXiv e-prints, arXiv:2408.06626